Plant plasmodesmata bridges form through ER-driven incomplete cytokinesis

Ziqiang P. Li[1]†‡*, Hortense Moreau[1]†, Jules D. Petit[1], Tatiana Souza-Moraes[1], Marija Smokvarska[1], Jessica Perez-Sancho[1], Melina Petrel[2], Fanny Decoeur[2], Lysiane Brocard[2], Clément Chambaud[1,2], Magali Grison[1], Andrea Paterlini[1]§, Lucie Hoornaert[1], Amit S. Joshi[3], Etienne Gontier[2], William A. Prinz[4], Yvon Jaillais[5], Antoine Taly[6], Felix Campelo[7], Marie-Cécile Caillaud[5], Emmanuelle M. Bayer[1]*

[1] Laboratoire de Biogenèse Membranaire, UMR5200, CNRS, Université de Bordeaux; Villenave d'Ornon, France.
[2] Bordeaux Imaging Centre, UMS 3420, INRA-CNRS-INSERM-University of Bordeaux; Bordeaux, France.
[3] Department of Biochemistry and Cell and Molecular Biology, University of Tennessee; Knoxville, USA.
[4] Department of Cell Biology, Medical School, UT Southwestern Medical Center, University of Texas, Dallas, USA
[5] Laboratoire Reproduction et Développement des Plantes, Université de Lyon, ENS de Lyon, UCB Lyon 1, CNRS, INRAE; F-69342 Lyon, France.
[6] Laboratoire de Biochimie Théorique, UPR9080, CNRS, Université Paris Cité; Paris, France.
[7] ICFO-Institut de Ciencies Fotoniques, The Barcelona Institute of Science and Technology, Barcelona, Spain.

‡ Present address: Institute of Science and Technology Austria (ISTA), Klosterneuburg, Austria
§ Present address: Institute of Molecular Plant Sciences, School of Biological Sciences, University of Edinburgh, Edinburgh EH9 3BF, UK.

† These authors contributed equally to this work
* Corresponding authors. Email: ziqiang.li@ist.ac.at (Z.P.L.); emmanuelle.bayer@u-bordeaux.fr (E.M.B)

Abstract: Diverging from conventional cell division models, plant cells undergo incomplete division to generate plasmodesmata communication bridges between daughter cells. While fundamental for plant multicellularity, the mechanisms governing bridge stabilization, as opposed to severing, remain unknown. We found that the endoplasmic reticulum (ER) is decisive in promoting incomplete cytokinesis by inhibiting local abscission events. ER tubes within contracting cell plate fenestrae create energy barriers preventing full closure. Contraction ceases upon encountering a metastable ER-plasma membrane tubular structure, leading to plasmodesmata formation. This process relies on the ER-tethers multiple C2 domains and transmembrane domain proteins 3, 4, and 6, which act as ER stabilizers, preserving ER position and integrity in nascent bridges. Our findings unveil the mechanisms through which plants undergo incomplete division to promote intercellular communication.

One-Sentence Summary: Uninterrupted ER connections obstruct abscission, causing incomplete cytokinesis and plasmodesmata formation in plants.

Main Text:

Intercellular bridges arising from incomplete cytokinesis act as structural mediators of clonal multicellularity, enabling daughter cells to communicate (*1*, *2*). These cytoplasmic connections have independently emerged across the eukaryotic tree of life spanning from animals to fungi (*3*–*8*). Their origin lies in the incomplete separation of daughter cells, wherein the "final cut" or abscission, responsible for severing membrane and cytosolic continuity, is impeded. Consequently, sibling cells maintain cytoplasmic bridges, forming a syncytium-like structure. While incomplete cytokinesis is cell-type specific in animals and results in a single cytoplasmic bridge (*9*), plants systematically employ this strategy to build up their communication network, creating not one but several hundreds of cytoplasmic plasmodesmata bridges, between daughter cells (**Fig. 1 A-H**). These bridges are maintained post-cytokinesis and are the foundation for generating a multicellular communication network, indispensable for plant life (*3*, *10*–*18*).

Land plants' cytokinesis differs significantly from animals. In animals, cytokinesis involves furrowing until daughter cells remain connected by a thin intercellular plasma membrane bridge (*1*, *19*, *20*). The transition from abscission to bridge stabilization requires ubiquitination of the ESCRT-III (endosomal sorting complex required for transport III) machinery (*21*). In higher plant cytokinesis, a disk-shaped membrane compartment called the cell plate, expands, eventually becoming the future plasma membrane and cell wall that will separate the daughter cells (*22*–*25*) (**Fig. 1A**). As the cell plate forms it is punctured by numerous fenestrae (see fenestrated-sheet stage, **Fig. 1A**) that by the end of the cytokinesis (hypothetically at cross-wall stage, **Fig. 1A**) will either be stabilized into plasmodesmata bridges or presumably sealed off, hinting at a yet-to-be-identified molecular switch. While cytoplasmic bridge formation traditionally involves mechanisms that prevent membrane abscission between daughter cells (*21*), the mechanisms underlying bridge stabilization in plants remain unexplored. We do not know how incomplete cytokinesis is achieved and how decision-making between abscission or bridge stabilization is regulated. Here, we investigated the fundamental question of how plant cells connect while dividing, using *Arabidopsis thaliana* root meristem, as an experimentally tractable model for plant cell division.

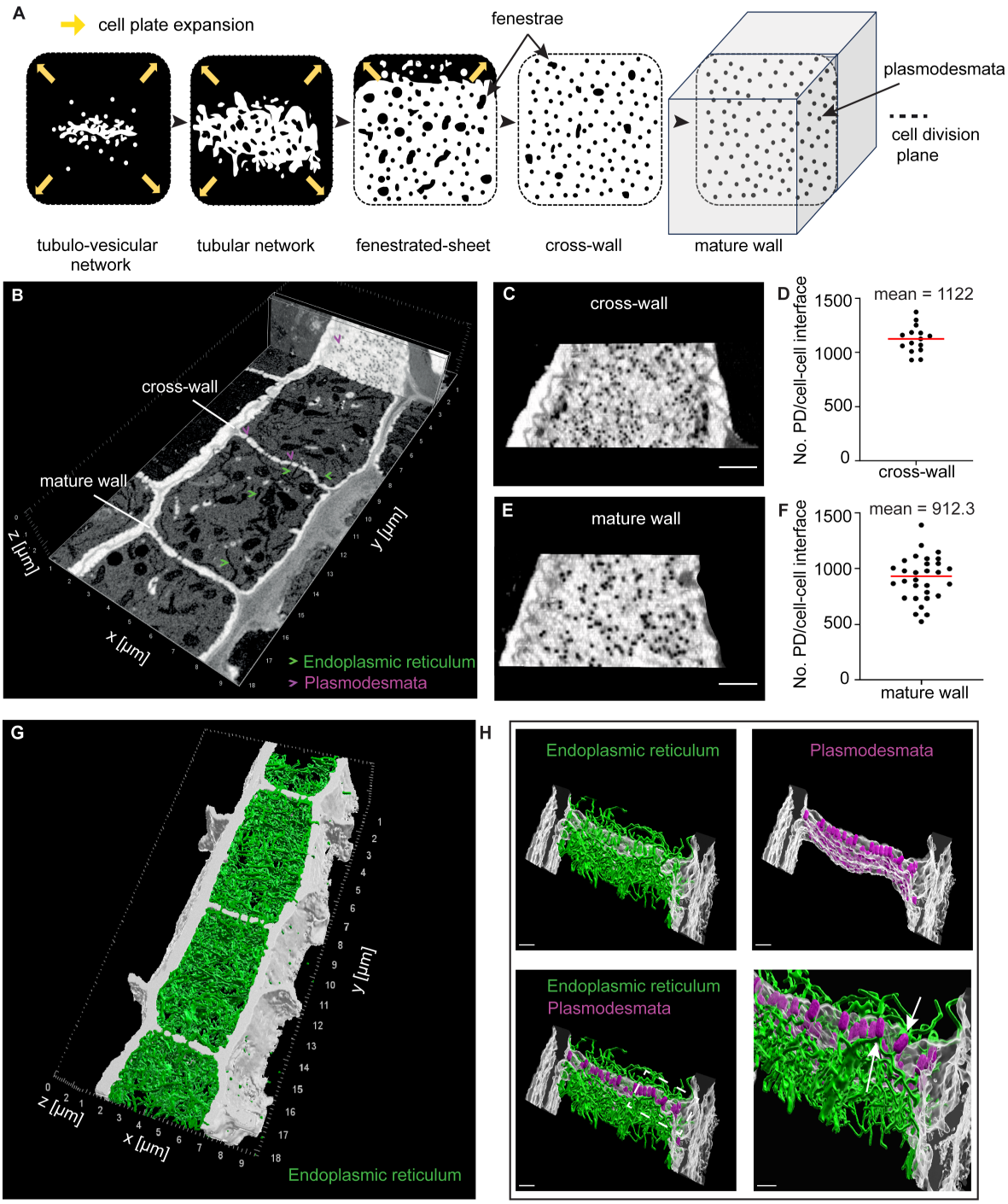

Fig. 1. Plasmodesmata formation and ER cell-cell continuity via incomplete cytokinesis in Arabidopsis. (**A**) Schematic representation of cell plate formation during cytokinesis. (**B**) SBF-SEM image of 4-day-old *Arabidopsis thaliana* root endodermis dividing cells. (**C, E**) Orthogonal projection of a section of cross-wall (C) and mature wall (E) from B, showing plasmodesmata as black holes in the division wall (incomplete cytokinesis). (**D, F**) Plasmodesmata quantification in cross-walls (D) and mature walls (F), n = 15 and n = 30, respectively. (**G**) 3D segmentation from SBF-SEM data in (B) illustrating ER (green) continuity through adjacent cells across plasmodesmata bridges. (**H**) Zoom on cross wall from (G) showing with ER continuity (white arrows) through plasmodesmata (magenta). Scale bar = 1µm (C, E); 0.5 µm (three first images of panel H) and 0.4 µm (for the last image of panel H).

ER continuity between daughter cells is build up early and maintained throughout cytokinesis across the division wall

An emblematic trait of plant cytokinesis lies in its capacity to preserve not just the continuity of the plasma membrane but also the continuity of the ER across division walls through plasmodesmata (*26*, *27*). Mitotic division creates a continuum of ER connections between daughter cells (**Fig. 1G-H, Movie S1**). Out of 126 plasmodesmata (n = 76 cross-wall, n = 50 mature wall) examined by scanning transmission electron microscopy (STEM) tomography in the division zone of the root, 120 plasmodesmata (n = 71 cross-wall, n = 49 mature wall) were confidently identified with an ER tube crossing through (**fig. S1, Movie S2**). While ER cell-cell continuity is a hallmark of plants, the ER's role in incomplete cytokinesis, its dynamics, integration into plasmodesmata bridges, and its connection to bridge stability remain unclear.

With this question in mind, we first determine how the ER network penetrates the forming cell wall during division. We first imaged live root meristem cells stably expressing the ER lumen (RFP-HDEL or YFP-HDEL (*28*)), cell plate/plasma membrane (PM) (Lti6b-GFP (*29*)) and microtubule (tagRFP-TUA5 (*30*)) markers. As the cells enter mitosis, the ER is excluded from mitotic spindles (**fig. S2A**) and overall, the ER pattern resembles that observed in other eukaryotes (*31*). However, starting from cytokinesis, the plant division scheme differs from animals and yeast, as membrane vesicles start gathering and fusing at the center of the division plane, and soon form the cell plate that expands centrifugally to finally partition the daughter cells (*24*, *25*). By simultaneously tracing cell plate vesicles (Lti6b-GFP) and the ER (RFP-HDEL), we observed early ER accumulation at the cell plate immediately upon vesicles starting to assemble at the division plane (**fig. S2B** and **Movie S3**). This tight association persisted throughout the entire cytokinetic process. To further explore the ER's organization in relation to the forming cell plate, we next utilized airyscan imaging (*32*). We observed ER strands crossing over the forming cell plate from the beginning to the end of the cytokinesis (**fig. S3 A-B**), resembling the dense ER intercellular matrix connecting post-cytokinetic cells (**Fig. 1A, G-H; Movie S1; fig. S1; Movie S2**). At early stages of cytokinesis, the ER was already one single and continuous compartment, stretching across the two daughter cells as demonstrated by fluorescence loss in photobleaching (FLIP) targeting the ER luminal marker (YFP-HDEL) (**fig. S3 C-D; Movie S4**). Thus, cell-cell ER continuity originates from early cytokinesis and is then persistent across the expanding cell plate.

ER tubules facilitate cytoplasmic bridge formation by elevating fenestrae sealing energy barrier during cell plate maturation

We then looked at the fate of the fenestrae in relation to the ER. It was previously hypothesized that during cell plate maturation fenestrae gradually shrink until a final stage where they either form plasmodesmata or are sealed off (*23*). This implies that one dividing cell can engage in both abscission and stabilization events while it progresses to the end of cytokinesis. To get insight into this decision-making process, we looked back at fenestrae events along the entire division plane using electron tomography (**Movie S5**). We focus on both fenestrated-sheet stage (when the cell plate forms a continuous membrane sheet) and cross-wall stage (when the cell plate has fused parental side walls) (**Fig. 1A**), when fenestrae are transitioned into the plasmodesmata (**Fig. 2A; fig. S4**). We employed chemically fixed and osmium ferricyanide-stained root meristem to specifically enhance ER staining and to be able to clearly visualize this membrane compartment

during cell plate formation (*27*). Altogether, we observed 118 fenestrae events by electron tomography from five and four cytokinetic cells for fenestrae-sheet and cross-wall stages respectively, providing a comprehensive and quantitative representation of plasmodesmata formation (**Fig. 2 and Fig. 3**). We noticed a marked disparity between the two stages regarding ER association with fenestrae. While at cross-wall stage, all fenestrae examined presented continuous ER, the preceding fenestrated-sheet stage displayed only 65.7% of events with clear ER physical continuity across fenestrae, while 11.8% showed ER association without cell-cell continuity and the remaining 22.5% showed no ER continuity with fenestrae sealing off (**Fig. 2B-C; Movies S6-8**).

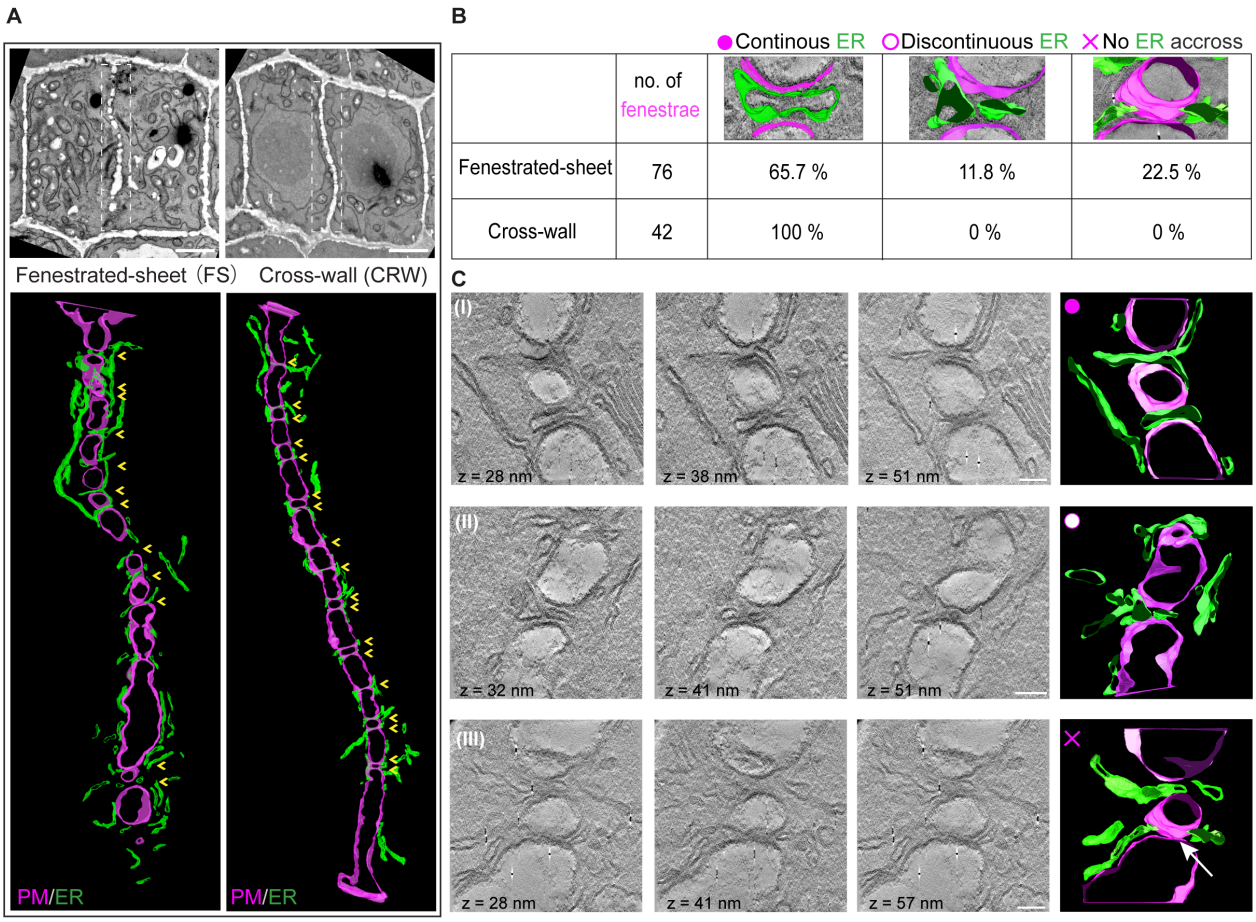

Fig. 2. Stabilized plasmodesmata bridges contain ER. (**A**) Batch electron tomography acquisitions along the entire cell plate at fenestrated-sheet (FS, n = 5) and cross-wall (CRW, n = 4) stages (top, overview of the dividing cells; bottom 3D segmentation of the cell plate for stitched tomograms). Cell plate membrane (PM) in magenta, ER in green, yellow arrows point to fenestrae. (**B**) Quantification of fenestrae events presenting continuous ER across, discontinuous ER across or no ER across at fenestrated-sheet and cross-wall stage. n = 76 fenestrae for FS (five complete cell plates) and n = 42 fenestrae for CRW (four complete cell plates). (**C**) Reconstructed tomography sections across fenestrae events and 3D segmentation showing: (I) open fenestrae with continuous ER; (II) open fenestrae with discontinuous ER and (III) closing fenestrae with ER structures flanking the fusion site. Scale bars, 2 μm (A); 100 nm (C).

We therefore asked whether steady positioning of ER tubes across fenestrae could somehow stabilization of plasmodesmata bridges. To understand the biophysical mechanisms behind this process, we built a semi-quantitative physical and computational model of plasmodesmata-fenestrae morphology and energetics. Our model computes the free energy of the system, which in our case corresponds to a single bridge, and includes the contributions of *i)* the cell plate (membrane bending energy and lateral tension, turgor pressure, and a force associated to the expansion of the cell plate, and *ii)* the ER (tubule bending energy, lateral tension, hydration repulsion between the two membranes) (see Methods for a detailed discussion of the different free energy terms and parameters). The outputs of the model indicate that expansion of the cell plate energetically favors fenestrae shrinking. However, the presence of the ER increases the energy barrier (that of membrane fusion or membrane tube removal) against complete sealing and allows fenestrae to reach an energetically metastable state with a predicted diameter of 19.5 nm (**Fig. 3A**).

To compare our experimental data with the model prediction, we systematically correlated the size of fenestrae with the ER in its various states (continuous, discontinuous, no ER) across both fenestrated-sheet and cross-wall stages (**Fig.3 B-E**). We indeed observed contraction of fenestrae as the cell plate mature (**Fig. 3 C-E**). At fenestrated-sheet stage, fenestrae diameter spans from 301.2 nm to below 10 nm. By the end of cytokinesis (cross-wall stage), fenestrae had stabilized to a uniform diameter of 22.3 ± 5.8 nm (mean ± SD) (**Fig. 3 C; fig. S1**), a value very close to the model's prediction (19.5 nm, **Fig. 3A)**. The stabilization of contracting fenestrae into metastable plasmodesmata bridges was invariably associated with the presence of ER in a contracted form (**Fig. 3 D; fig. S1**). In the absence of the ER, fenestrae diameter decreases below 20 nm until complete closure (as they are not present in cross-wall stage) (**Fig. 3 E**). From these data we concluded that the ER's presence works against full fenestrae closure, explaining why stabilized cytoplasmic bridges always include ER and present a steady diameter.

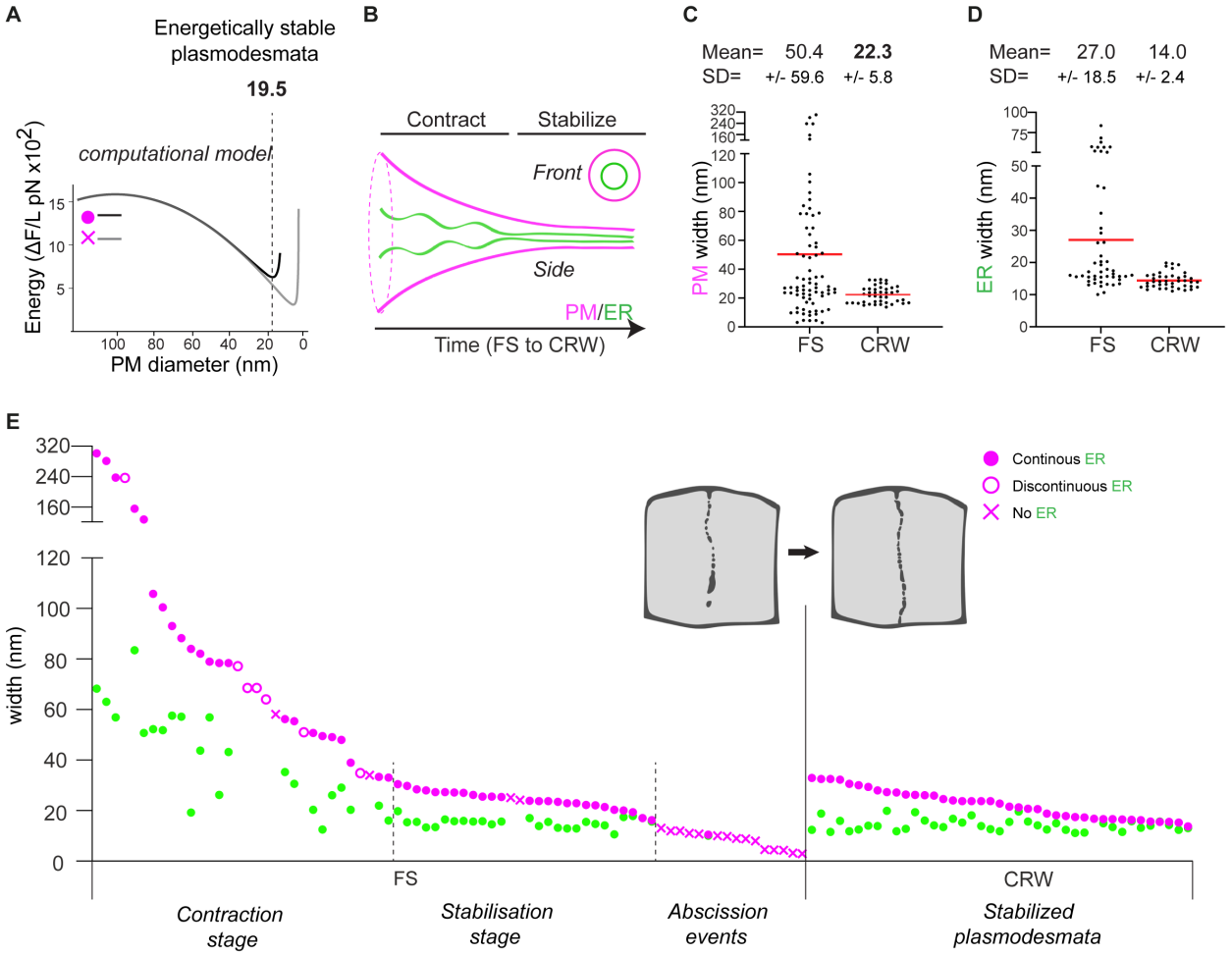

Fig. 3. The ER creates an energy barrier preventing full fenestrae closure. (**A**) Computational model of energetically metastable plasmodesmata. The presence of ER works against full fenestrae closure (PM sealing) by creating an extra energy barrier (that of ER removal), leading to metastable structure of about 19.5 nm in diameter (ΔF, free energy of the structure. L, longitudinal length of the fenestrae). (**B**) Schematic model of fenestrae contraction and stabilization during cytokinesis from fenestrated-sheet (FS) to cross-wall (CRW) stages. PM term is used for the cell plate membrane. (**C**) Diameter of ER tubes across fenestrae at FS and CRW stages. n = 50 for FS and n = 41 for CRW extracted from electron tomography acquisition from Fig.2. (**D**) Diameter of fenestrae (PM) at FS and CRW stage, n = 76 for FS and n = 42 for CRW extracted from electron tomography acquisition from Fig.2. (**E**) Plotting of fenestrae (PM) diameters together with ER state (continuous, discontinuous, absence, and diameter) during FS and CRW stages.

The ER-associated MCTP3, 4, 6 tethers are key elements of plasmodesmata bridge formation

Our data indicates a critical role for the ER in the generation of metastable plasmodesmata bridges. Given the highly dynamic nature of this compartment specific factors are likely necessary for retaining the ER across contracting fenestrae. We therefore looked for proteins that can stabilize the ER while plasmodesmata form.

Previously, we identified a plasmodesmata-specific ER protein family named multiple C2 domains and transmembrane proteins (MCTPs), whose function is predicted to hold the ER proximal to the

plasma membrane (PM) inside plasmodesmata (*33*). MCTPs are one of the very few plasmodesmata-enriched ER proteins identified so far, and were recently proposed to be core structural elements of plasmodesmata (*33–35*), making them strong candidates. Based on single cell RNA-sequencing analysis (*36*), out of 16 members in *Arabidopsis*, four members are particularly expressed in dividing cells, with MCTP3, MCTP4, and MCTP6 showing ubiquitous transcription in the root meristematic cells (**fig. S5A**). When fluorescently-tagged MCTP3, MCTP4, and MCTP6 were expressed under endogenous promoters, they all showed localization to the ER/cell plate in dividing cells (**fig. S5B-D)**. They also appeared as dots, typical of plasmodesmata association, at cell-cell interfaces of newborn daughter cells which we confirmed by correlative light and electron microscopy (CLEM) for MCTP4 (**Fig. 4 A-B**). Post-cytokinesis, plasmodesmata are only 50-100 nm in length, making it hard to differentiate ER signals inside and outside. To tackle this, we employed airyscan microscopy, which revealed that the 'dotty' MCTP-fluorescent signals were actually stripes extending across the wall connecting sister cells (**Fig. 4C**). In contrast, synaptotagmin (SYT1 and SYT5), and reticulon (RTN 6) proteins involved in ER-PM tethering and ER shaping (*37*, *38*), respectively, were excluded from the cytokinetic bridges (**Fig. 4C**). These findings highlight the molecular specialization of ER within newborn cytokinetic-plasmodesmata, which are populated by MCTPs, providing us with the genetic targets to disturb the ER-PM contact within plasmodesmata and test our hypothesis that bridge stabilisation relies on the ER.

For that we generated *mctp* loss-of-function mutants and asked whether they present a defect in plasmodesmata production. As MCTP3 and MCTP4 share 98% protein homology and are functionally redundant (*33*), we focused on the double (*mctp3/mctp4*) and triple (*mctp3/mctp4/mctp6*) mutants. We first quantified plasmodesmata in newly formed post-cytokinetic division walls across four root cell layers (epidermis, cortex, endodermis and pericycle - apico-basal post-division walls) using transmission electron microscopy. Cytokinetic plasmodesmata are ubiquitous structures and essential factors for their formation should have a global impact across multiple cell types. We found that *mctp* mutants presented an important drop of plasmodesmata in all four layers examined (reflected as density, number per unit area, ranging from 28% drop in the cortex to 47% drop in the epidermis) (**fig. S6**) when compared to the wild-type. MCTP6 is down-regulated at the protein level in the *mctp3/mctp4* mutant (*33*), explaining the phenotypic similarity between *mctp3/mctp4* and *mctp3/mctp4/mctp6* genotypes. The reduced but not complete absence of plasmodesmata was expected considering the large MCTP multigenic family and the possible contribution of additional factors. While we speculated that the plasmodesmata phenotype in the *mctp* mutants originate from cytokinesis defects, selective removal of mature post-cytokinetic plasmodesmata cannot be ruled out. We reason that cytokinesis-defect should lead to a reduction in cross-wall and mature wall plasmodesmata, while post-cytokinesis elimination should affect mature walls only. To clarify this point, we took advantage of serial block-face scanning electron microscopy (SBF-SEM) to map plasmodesmata across the entire cell volume at cross-wall and mature wall stages (**fig. S7**). We focused on the endodermis due to its superior sample preservation. SBF-SEM data indicate that the plasmodesmata deficiency originated from cytokinesis as *mctp* mutants presented significantly fewer cytoplasmic bridges from cross-wall stage (**Fig. 4D-E**). Complementation of *mctp3/mctp4* mutant with a *UBQ10:YFP-MCTP4* transgene was sufficient to restore plasmodesmata to the wild-type level (two independent lines; **Fig. 4D-E**). Our results show that ER-associated MCTP tethers are needed for efficient plasmodesmata formation during cytokinesis.

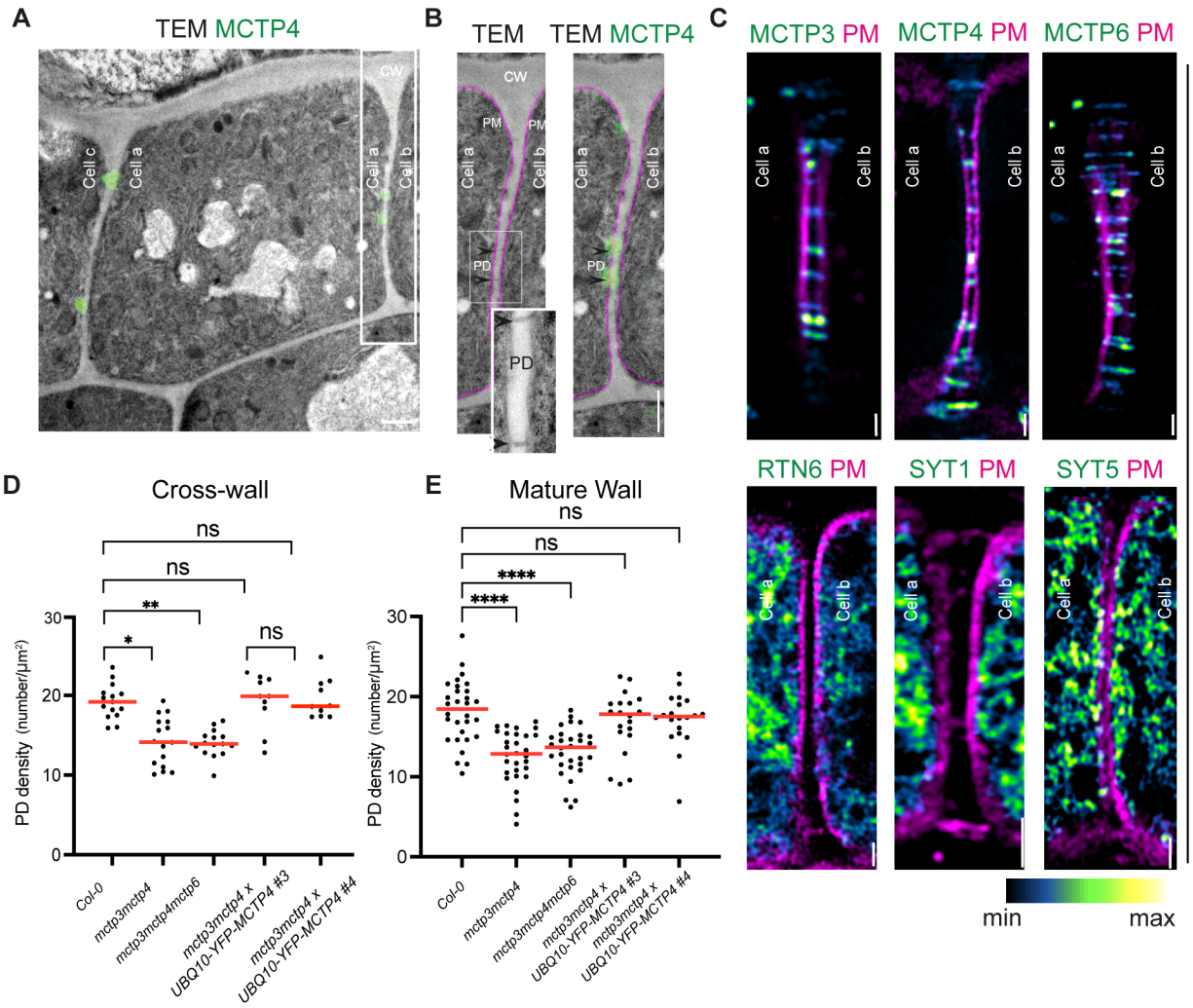

Fig. 4. MCTPs ER-tethers are necessary for plasmodesmata formation. (**A-B**) CLEM on YFP-MCTP4 expressed in genetically complemented *mctp3/mctp4* mutants in root meristem epidermal cells. (B) enlarged region as in A (outlined white rectangle). Black arrows point to the two plasmodesmata connecting cell a and cell b. Green: YFP-MCTP4; Magenta: PM; CW: cell wall; TEM: transmission electron microscopy. (**C**) airyscan imaging of live Arabidopsis meristem epidermal cells expressing YFP-tagged MCTP3, MCTP4, MCTP6, SYT1, STY5 (green fire blue) under their native promoter; RTN6 under 35S promoter. PM (magenta) is stained by FM4-64. (**D-E**) Quantification of plasmodesmata density on cross-walls and mature walls (number of plasmodesmata/µm^2) in the *A. thaliana* root meristem endodermis cells using SBF-SEM. The bars indicate the mean. Significance was tested using ordinary two tailed Mann-Whitney U-tests (****, P<0.0001). n = 15 (Col-0), n = 16 *(mctp3/mctp4)*, n = 15 (*mctp3/mctp4/mctp6*), n = 10 (*mctp3/mctp4 x UBQ10-YFP-MCTP4 line* #3), n = 10 (mctp3/mctp4 x UBQ10-YFP-MCTP4 line #4) cells for the cross-wall quantification. n = 30 (Col-0), n = 30 (*mctp3/mctp4*), n = 30 (*mctp3/mctp4/mctp6*), n = 20 (*mctp3/mctp4 x UBQ10-YFP-MCTP4* line #3), n = 20 (*mctp3/mctp4 x UBQ10-YFP-MCTP4* line #4) cells for the mature wall quantification. Scale bars, 1 µm (A, B, C, E) or 20 nm (F).

MCTPs target, oligomerize and shape the ER at contracting fenestrae, stabilizing cytoplasmic bridges against abscission

Next, we addressed the timing and the mechanism by which MCTPs contribute to plasmodesmata formation. Using live imaging, we first followed MCTP dynamics during cytokinesis in genetically complemented plants. MCTP3, 4 and 6 proteins initially showed a uniform distribution at the ER-associated cell plate, comparable to the general ER membrane marker cinnamate 4-hydroxylase C4H-GFP (*39*) (**Fig. 5A, fig. S8A-C**). However, just before cross-wall transition (annotated as t=0), YFP-MCTPs signal started to accumulate at nascent plasmodesmata, as confirmed by CLEM (**Fig. 5B**; six plasmodesmata out of two cross-wall cells), contrasting with C4H-GFP's uniform distribution. MCTPs clustering coincides with fenestrae stabilization into stable bridges (**Fig. 3**). At this stage, the cell plate membrane closely wraps around constricted ER (**fig. S1**), suggesting an interlink between ER-cell plate tethering and ER constriction. We therefore investigated if, in addition to their membrane tethering activity, MCTPs could also shape the ER. We found that the ER-anchor C-terminal region of MCTPs (transmembrane region, TMR), presents homology to the ER-shaping reticulon-domain (*40*), a function we experimentally confirmed *in planta* and in yeast (**Fig. 5C**, **fig. S9**). To determine the role of MCTP ER-shaping segment and C2 lipid-binding domains in targeting plasmodesmata, we created truncated MCTP4-TMR and MCTP4-C2 mutants with sequential sub-segment deletions (**fig. S10A**). Except for C2B deletion mutant, clustering at plasmodesmata was lost for all tested truncated mutants (**fig. S10B, C)**, suggesting that both the TMR domain (ER shaping) and C2 cytoplasmic domain (membrane tethering) are important for accumulation at nascent plasmodesmata.

The molecular machinery for abscission/stabilization in animals and yeast operates locally within the bridge, adopting a stationary matrix-like molecular organization (*19*, *41*). We speculated that MCTPs behave alike and investigated their mobility by fluorescence recovery after photobleaching (FRAP) and FLIP. These techniques complement each other, with FRAP showing the mobile protein fraction and its dynamics, while FLIP reveals the locations of non-mobile proteins by depleting the mobile population. All three MCTPs exhibited high-dynamic behavior before accumulating at nascent plasmodesmata (**Fig. 5D-E** and **fig. S11A-C**). However, from the cross-wall stage, their mobility dramatically decreased as indicated by FRAP, and in nascent-plasmodesmata associated MCTP signal persists under FLIP (**fig. S11D-E)**. In contrast, the ER membrane marker, C4H-GFP, remained highly mobile throughout cytokinesis (**fig. S11A**).

A straightforward explanation for the stable accumulation of MCTPs at contracting fenestrae during late cytokinesis is their organization in polymeric lattices. Such hypothesis is consistent with the presence of an RTN-homology domain known to induce oligomerization (*42*, *43*). Using co-immunoprecipitation, we show that all three MCTP RTN-homology domains can indeed physically interact (**fig. S12A**). To further test whether MCTPs are present as oligomeric complexes, we extracted YFP-MCTP4 (from *A. thaliana mctp3/mctp4* complemented lines) from plasmodesmata-enriched wall fractions under native extraction conditions, using non-denaturing native-blue gel. The majority of YFP-MCTP4 (120kD as monomer) was detected as a complex of about 1000 kDa regardless of the non-ionic detergents used (**Fig 5F**, **fig. S12B-C**). Strikingly, YFP-MCTP4 high-molecular-weight complexes resisted strong disruptive SDS/DTT solubilization conditions (**fig. S12D-E**). We concluded that plasmodesmata-enriched MCTPs form highly stable oligomer complexes.

Based on our observations, we hypothesized that ER-associated MCTPs concentrate at fenestrae ingression sites, where they oligomerize, stabilizing ER strands across nascent bridges and forming a protective shield to prevent abscission. In this scenario, loss of MCTPs would shift the balance

towards abscission, explaining the loss of plasmodesmata (**Fig. 4D-E, fig. S6**). To test this hypothesis, we went back to our semi-quantitative physical model of plasmodesmata formation, and incorporated MCTPs taking into account the entropic contribution of MCTP concentration, the adhesion energy between the ER and the cell plate membrane mediated by MCTP tethering activity, and MCTP-ER shaping activity (see Methods for detailed parameters). The model's outcome indicates that the enrichment of MCTPs in contracting fenestrae is energetically favorable. This sorting effect arises from both the curvature-generating/sensing characteristics of the RTN-homology domain and the contact-driven sorting through tethering activity (**Fig. 5G, fig. S13**). As previously mentioned, the presence of an ER tubule, within narrowing fenestrae, creates an energy barrier (that of ER tubule fission or ER-tubule removal) working against fenestrae closure. MCTPs introduce an extra obstacle compared to the ER alone, hindering complete closure and leading to the formation of metastable ER-cell plate membrane bridges. Collectively, our data support a spatio-temporal coordination model, wherein MCTPs concentrate at fenestrae ingression sites to assist the ER's action and establish stable communication bridges (**Fig. 5H**).

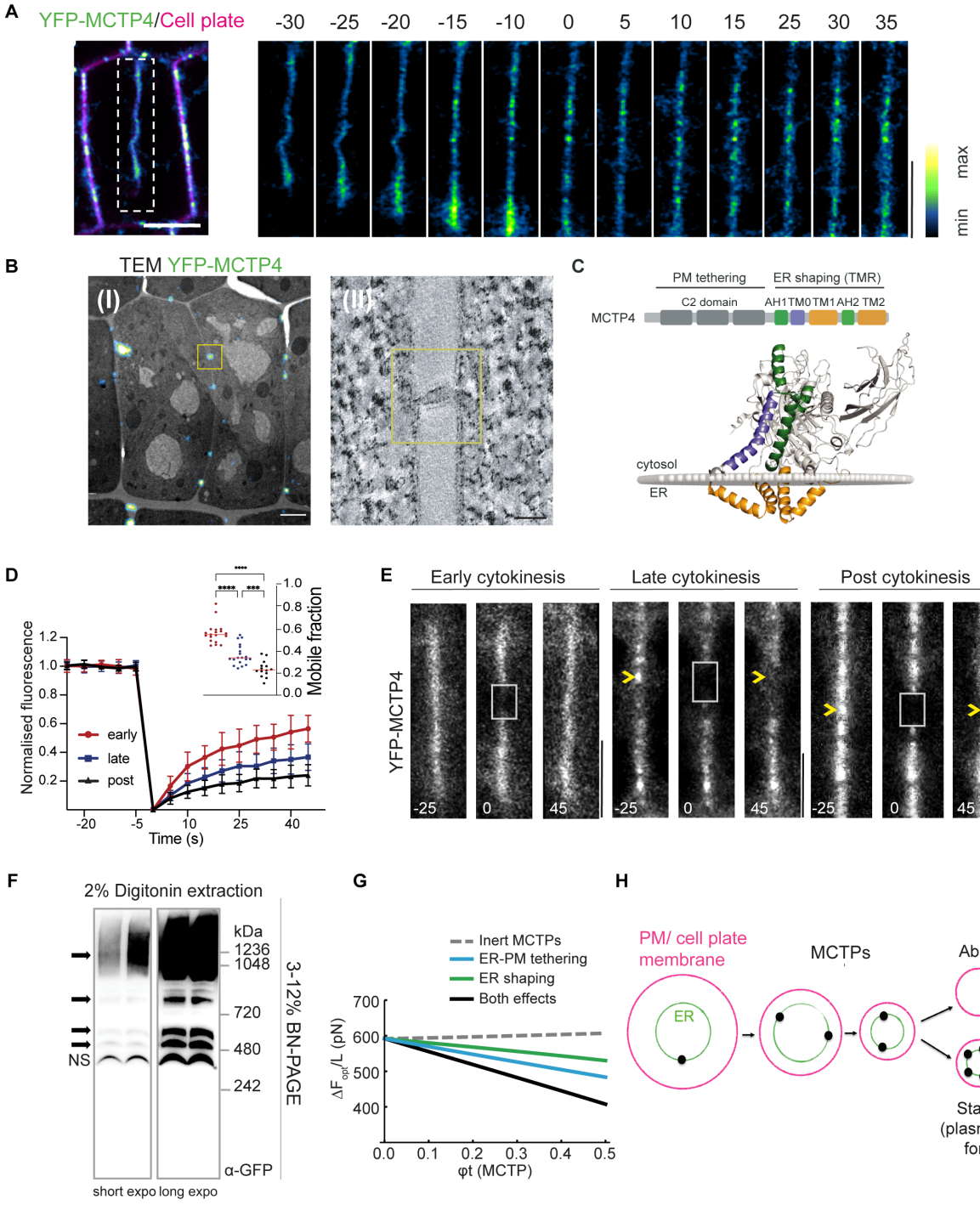

Fig 5. MCTPs accumulate and oligomerize within nascent plasmodesmata late cytokinesis to prevent abscission. (**A**) YFP-MCTP4 time lapse during cytokinesis in the *mctp3/mctp4* complemented *A. thaliana* seedling root epidermal cells. Time 0 indicates the start of cross-wall stage. Note MCTP4 signal starts to accumulate as dots at the onsite of the cross-wall stage. MCTP4 in color coded green fire blue and cell plate in magenta (FM4-64). (**B**) Analyzed by CLEM, YFP-MCTP 'dots' (I) correspond to nascent plasmodesmata (II). (**C**) MCTP4 domain organization and 3D structure. (**D-E**) YFP-MCTP4 mobility during early, late cytokinesis and post cytokinesis, measured by fluorescence recovery after photobleaching (FRAP) in root epidermal dividing cells from *mctp3/mctp4* complemented line. The white squares indicate the photobleaching regions at t = 0. Yellow arrows indicate MCTP4 'dots' that does not recover fluorescent

signal after photobleaching. Time is shown in second. Quantification of fluorescence (mean ± SD) and mobile fraction (bars indicate mean) in n = 19 (early cytokinesis) and n = 19 (late cytokinesis) dividing cells. Significance was tested using ordinary two tailed Mann-Whitney U-tests (****, P<0.0001). (**F**) YFP-MCTP4, extracted by digitonin, oligomerizes *in vivo*, as shown by 3-12 % Blue native-PAGE gel. Black arrows point to MCTP4 high-molecular weight complexes in both short (51 s) and long exposed (157 s) blots. Non-specific (NS) indicates non-specific band. Representative results from 3 technical replicates. (**G**) Enrichment of MCTP (ϕ_t=fraction of MCTP covering the ER surface) further stabilizes nascent plasmodesmata bridges by reducing the free energy of the system, which both and depends on both their tethering and ER shaping functions. (**H)** Recapitulative schema. Molecular decision making between abscission and stabilization of constricting fenestrae into plasmodesmata bridges come from the ER and ER-associated MCTPs. Scale bars, 5 µm (A and E), 50 nm (B I, II).

Conclusion

In this study, we identified a novel function of the ER in preventing cytokinetic abscission in plants, leading to the formation of stable intercellular bridges. Abscission and stabilization events occur concurrently during the same cytokinetic event, and the switch between the two is governed by the ER along with MCTP proteins (**Fig. 5H**). During cytokinesis, the ER permeates the cell plate, maintaining contact across closing fenestrae and recruiting MCTPs to prevent closure, thereby stabilizing the bridge in a metastable configuration that persists after cytokinesis. Without MCTPs, ER physical continuity across contracting fenestrae is lost and plasmodesmata formation is compromised. Our observations resolve the longstanding puzzle regarding the presence of ER inside plasmodesmata and highlights the necessity for intercellular ER continuity. Last, the mechanism of local ER remodeling sheds light on incomplete cytokinesis and offers a comparison for stable intercellular bridge formation in other eukaryotes.

References

1. A. Chaigne, T. Brunet, Incomplete abscission and cytoplasmic bridges in the evolution of eukaryotic multicellularity. *Curr. Biol.* **32**, R385–R397 (2022).
2. A. C. Spradling, The ancient origin and function of germline cysts. *Results Probl. Cell Differ.* **71**, 3–21 (2024).
3. J. O. Brunkard, P. C. Zambryski, Plasmodesmata enable multicellularity: new insights into their evolution, biogenesis, and functions in development and immunity. *Curr. Opin. Plant Biol.* **35**, 76–83 (2017).
4. S. K. Ong, C. Tan, Germline cyst formation and incomplete cytokinesis during Drosophila melanogaster oogenesis. *Dev. Biol.* **337**, 84–98 (2010).
5. P. F. McLean, L. Cooley, Protein equilibration through somatic ring canals in Drosophila. *Science.* **340**, 1444–1447 (2013).
6. M. Terauchi, C. Nagasato, T. Motomura, Plasmodesmata of brown algae. *J. Plant Res.* **128**, 7–15 (2014).
7. T. Bisalputra, J. R. Stein, The development of cytoplasmic bridges in volvox aureus. *Can. J. Bot.* **44**, 1697–1702 (1966).
8. L. I. Rathbun *et al.*, Cytokinetic bridge triggers de novo lumen formation in vivo. *Nat. Commun.* **11** (2020), doi:10.1038/s41467-020-15002-8.
9. P. P. D'Avino, M. G. Giansanti, M. Petronczki, Cytokinesis in animal cells. *Cold Spring Harb.*

Perspect. Biol. **7**, a015834 (2015).

10. M. Kitagawa, P. Wu, R. Balkunde, P. Cunniff, D. Jackson, An RNA exosome subunit mediates cell-to-cell trafficking of a homeobox mRNA via plasmodesmata. *Science.* **375**, 177–182 (2022).

11. G. Daum, A. Medzihradszky, T. Suzaki, J. U. Lohmann, A mechanistic framework for non-cell autonomous stem cell induction in Arabidopsis. *Proc. Natl. Acad. Sci. U. S. A.* **111**, 14619–24 (2014).

12. S. Tylewicz *et al.*, Photoperiodic control of seasonal growth is mediated by ABA acting on cell-cell communication. *Science.* **360**, 212–215 (2018).

13. N. P. Nakajima, Keiji, Sena, G., Nawy, Tal, Benfey, Intercellular movement of the putative transcription factor SHR in root patterning. *Nature*. **413**, 307–311 (2001).

14. P. Mehra *et al.*, Hydraulic flux–responsive hormone redistribution determines root branching. *Science.* **378**, 762–768 (2022).

15. E. E. Tee, M. G. Johnston, D. Papp, C. Faulkner, A PDLP-NHL3 complex integrates plasmodesmal immune signaling cascades. *PNAS.* **120**, e2216397120 (2022).

16. R. Sager *et al.*, Auxin-dependent control of a plasmodesmal regulator creates a negative feedback loop modulating lateral root emergence. *Nat. Commun.* **11**, 1–10 (2020).

17. X. Han *et al.*, Auxin-callose-mediated plasmodesmal gating is essential for tropic auxin gradient formation and signaling. *Dev. Cell*. **28**, 132–146 (2014).

18. R. Gaudioso-Pedraza *et al.*, Callose-regulated symplastic communication coordinates symbiotic root nodule development. *Curr. Biol.* **28**, 3562-3577.e6 (2018).

19. J. Guizetti *et al.*, Cortical constriction during abscission involves helices of ESCRT-III-dependent filaments. *Science.* **331**, 1616–1620 (2011).

20. J. Lafaurie-Janvore *et al.*, ESCRT-III Assembly and Cytokinetic Abscission Are Induced by Tension Release in the Intercellular Bridge. *Science.* **339**, 1625–1629 (2013).

21. J. Mathieu, P. Michel-Hissier, V. Boucherit, J.-R. Huynh, The deubiquitinase USP8 targets ESCRT-III to promote incomplete cell division. *Science.* **376**, 818–823 (2022).

22. A. Smertenko *et al.*, Plant cytokinesis: terminology for structures and processes. *Trends Cell Biol.* **27** (2017), pp. 885–894.

23. J. M. Seguí-Simarro, J. R. Austin, E. A. White, L. A. Staehelin, Electron tomographic analysis of somatic cell plate formation in meristematic cells of Arabidopsis preserved by high-pressure freezing. *Plant Cell*. **16**, 836–856 (2004).

24. G. Jürgens, Cytokinesis in higher plants. *Annu. Rev. Plant Biol.* **56** (2005), pp. 281–299.

25. P. Livanos, S. Müller, Division Plane Establishment and Cytokinesis. *Annu. Rev. Plant Biol*. **70**, 239–267 (2019).

26. W. Nicolas *et al.*, Architecture and permeability of post-cytokinesis plasmodesmata lacking cytoplasmic sleeve. *Nat. Plants*. **3**, 17082 (2017).

27. P. K. Hepler, "Endoplasmic reticulum in the formation of the cell plate and plasmodesmata" (1982).

28. C. Pain, V. Kriechbaumer, M. Kittelmann, C. Hawes, M. Fricker, Quantitative analysis of plant ER architecture and dynamics. *Nat. Commun.* **10**, 1–15 (2019).

29. A. Martiniere *et al.*, Cell wall constrains lateral diffusion of plant plasma-membrane proteins. *Proc. Natl. Acad. Sci.* **109**, 12805–12810 (2012).

30. S. Komaki, A. Schnittger, The spindle assembly checkpoint in Arabidopsis is rapidly shut off during

severe stress. *Dev. Cell*. **43**, 172-185.e5 (2017).

31. J. G. Carlton, H. Jones, U. S. Eggert, Membrane and organelle dynamics during cell division. *Nat. Rev. Mol. Cell Biol.* **21** (2020), pp. 151–166.

32. X. Wu, J. A. Hammer, ZEISS Airyscan:Optimizing usage for fast, gentle, super resolution imaging in *Methods in Molecular Biology* (2021), vol. 2304, pp. 111–130.

33. M. L. Brault *et al.*, Multiple C2 domains and transmembrane region proteins (MCTP) tether membranes at plasmodesmata. *EMBO Rep.* **e47182**, 1–26 (2019).

34. M. G. Johnston *et al.*, Comparative phyloproteomics identifies conserved plasmodesmal proteins. *J. Exp. Bot.* **74**, 1821–1835 (2023).

35. M. Miras *et al.*, Plasmodesmata and their role in assimilate translocation. *J. Plant Physiol.* **270** (2022), p. 153633.

36. J. R. Wendrich *et al.*, Vascular transcription factors guide plant epidermal responses to limiting phosphate conditions. *Science.* **370** (2020),.

37. N. Ruiz-Lopez *et al.*, Synaptotagmins at the endoplasmic reticulum–plasma membrane contact sites maintain diacylglycerol homeostasis during abiotic stress. *Plant Cell*. **33**, 2431–2453 (2021).

38. K. Knox *et al.*, Putting the Squeeze on Plasmodesmata: A Role for Reticulons in Primary Plasmodesmata Formation. *Plant Physiol.* **168**, 1563–72 (2015).

39. E. Lee *et al.*, Ionic stress enhances ER – PM connectivity via site expansion in Arabidopsis. *PNAS*. **116**, 1420–1429 (2019).

40. G. K. Voeltz, W. a. Prinz, Y. Shibata, J. M. Rist, T. a. Rapoport, A class of membrane proteins shaping the tubular endoplasmic reticulum. *Cell*. **124**, 573–586 (2006).

41. H. C. Nguyen *et al.*, Membrane constriction and thinning by sequential ESCRT-III polymerization. *Nat. Struct. Mol. Biol.* **27**, 392–399 (2020).

42. Y. Xiang, R. Lyu, J. Hu, Oligomeric scaffolding for curvature generation by ER tubule-forming proteins. *Nat. Commun.* **14** (2023), doi:10.1038/s41467-023-38294-y.

43. Y. Shibata *et al.*, The reticulon and Dp1/Yop1p proteins form immobile oligomers in the tubular endoplasmic reticulum. *J. Biol. Chem.* **283**, 18892–18904 (2008).

44. T. L. Shimada, T. Shimada, I. Hara-Nishimura, A rapid and non-destructive screenable marker, FAST, for identifying transformed seeds of Arabidopsis thaliana: *Plant J.* **61**, 519–528 (2010).

45. S. J. Clough, A. F. Bent, Floral dip : a simplified method for Agrobacterium-mediated transformation of Arabidopsis thaliana. *Plant J.* **16**, 735–743 (1998).

46. C. Chambaud, S. J. Cookson, N. Ollat, E. Bayer, L. Brocard, A correlative light electron microscopy approach reveals plasmodesmata ultrastructure at the graft interface. *Plant Physiol.* **188**, 44–55 (2022).

47. A. S. Joshi *et al.*, Lipid droplet and peroxisome biogenesis occur at the same ER subdomains. *Nat. Commun.* **9** (2018), doi:10.1038/s41467-018-05277-3.

48. J. Jumper *et al.*, Highly accurate protein structure prediction with AlphaFold. *Nature*. **596**, 583 (2021).

49. M. A. Lomize, I. D. Pogozheva, H. Joo, H. I. Mosberg, A. L. Lomize, OPM database and PPM web server: Resources for positioning of proteins in membranes. *Nucleic Acids Res.* **40** (2012), doi:10.1093/nar/gkr703.

50. C. Gaboriaud, V. Bissery, T. Benchetrit, J. P. Mornon, Hydrophobic cluster analysis: An efficient

new way to compare and analyse amino acid sequences. *FEBS Lett.* **224**, 149–155 (1987).

51. D. W. A. Buchan, F. Minneci, T. C. O. Nugent, K. Bryson, D. T. Jones, Scalable web services for the PSIPRED Protein Analysis Workbench. *Nucleic Acids Res.* **41**, W349-357 (2013).

52. R. Gautier, D. Douguet, B. Antonny, G. Drin, HELIQUEST: A web server to screen sequences with specific α-helical properties. *Bioinformatics*. **24**, 2101–2102 (2008).

53. W. Helfrich, Elastic properties of lipid bilayers: theory and possible experiments. *Zeitschrift fur Naturforsch.* **28**, 693–703 (1973).

54. R. Dharan *et al.*, Transmembrane proteins tetraspanin 4 and CD9 sense membrane curvature. *Proc. Natl. Acad. Sci. U. S. A.* **119**, e2208993119 (2022).

55. B. Zucker, G. Golani, M. M. Kozlov, Model for ring closure in ER tubular network dynamics. *Biophys. J.* **122**, 1974–1984 (2023).

56. J. Zimmerberg, M. M. Kozlov, How proteins produce cellular membrane curvature. *Nat. Rev. Mol. Cell Biol.* **7** (2006), pp. 9–19.

57. T. Shemesh, A. Luini, V. Malhotra, K. N. J. Burger, M. M. Kozlov, Prefission constriction of Golgi tubular carriers driven by local lipid metabolism: a theoretical model. *Biophys. J.* **85**, 3813–3827 (2003).

58. A. Goetz, Introduction to differential geometry. *Addison Wesley* (1972).

59. R. P. Rand, V. A. Parsegian, Physical force considerations in model and biological membranes. *Can. J. Biochem. Cell Biol.* **62**, 752–759 (1984).

60. S. L. Leikin, M. M. Kozlov, L. V. Chernomordik, V. S. Markin, Y. A. Chizmadzhev, Membrane fusion: overcoming of the hydration barrier and local restructuring. *J. Theor. Biol.* **129**, 411–425 (1987).

61. F. Campelo, H. T. McMahon, M. M. Kozlov, The hydrophobic insertion mechanism of membrane curvature generation by proteins. *Biophys. J.* **95**, 2325–2339 (2008).

62. S. Aimon *et al.*, Membrane Shape Modulates Transmembrane Protein Distribution. *Dev. Cell*. **28**, 212–218 (2014).

63. C. L. C. L. Thomas, E. M. Bayer, C. Ritzenthaler, L. Fernandez-Calvino, A. J. A. J. Maule, Specific targeting of a plasmodesmal protein affecting cell-to-cell communication. *PLoS Biol.* **6**, 0180–0190 (2008).

64. M. Z. Jawaid, R. Sinclair, V. Bulone, D. L. Cox, G. Drakakaki, A biophysical model for plant cell plate maturation based on the contribution of a spreading force. *Plant Physiol.* **188**, 795–806 (2022).

65. K. Park, J. Knoblauch, K. Oparka, K. H. Jensen, Controlling intercellular flow through mechanosensitive plasmodesmata nanopores. *Nat. Commun.* **10** (2019), doi:10.1038/s41467-019-11201-0.

66. G. Niggemann, M. Kummrow, W. Helfrich, The bending rigidity of phosphatidylcholine bilayers: dependences on experimental method, sample cell sealing and temperature. *J. Phys.* **5**, 413–425 (1995).

67. P. Sens, J. Plastino, Membrane tension and cytoskeleton organization in cell motility. *J. Phys. Condens. Matter*. **27** (2015), p. 273103.

68. V. Kriechbaumer, F. Brandizzi, The plant endoplasmic reticulum: an organized chaos of tubules and sheets with multiple functions. *J. Microsc.* **280**, 122–133 (2020).

69. A. Upadhyaya, M. P. Sheetz, Tension in tubulovesicular networks of golgi and endoplasmic reticulum membranes. *Biophys. J.* **86**, 2923–2928 (2004).

70. B. A. Lewis, D. M. Engelman, Lipid bilayer thickness varies linearly with acyl chain length in fluid phosphatidylcholine vesicles. *J. Mol. Biol.* **166** (1983), pp. 211–217.

Acknowledgments: We would like to thank Kevin Verstaen from the Vlaams Instituut voor Biotechnologie single cell core who provided the single cell sequencing raw data, which we used in the fig. S5. Sofia Otero provided the MCTP6 native reporter line. We thank Sebastian Marais for the help with iMaris software. Guillaume Maucort for the suggestions on the SBF-SEM visualization. Fabrice Cordelières for live-imaging data display. We would also like to thank Maya Schuldiner, Patricia Bassereau, Olivier Hamant, Agathe Chaigne, Thibaut Brunet, Yohann Boutté, Sébastien Mongrand for reading and commenting on the article. All light and electron imaging were done at the Bordeaux Imaging Center, member of the national infrastructure France-BioImaging supported by the French National Research Agency (ANR-10-INBS-04).

Funding: This work was supported by the European Research Council (ERC) under the European Union's Horizon 2020 research and innovation program (project 772103-BRIDGING to E.M.B.); the National Agency for Research (Grant ANR PRPC - ANR-21-CE13-0016-01 DIVCON, E.M.B, M.C.C.); the Human Frontier Research program (project RGP0002/2020, E.M.B.); the French government in the framework of the IdEX Bordeaux University "Investments for the Future" program / GPR Bordeaux Plant Sciences (E.M.B.); the Belgian "Formation a` la Recherche dans l'Industrie et l'Agriculture" (FRIA grant no. 1.E.096.18, J.D.P.).

Author contributions:

Conceptualization: Z.P.L, E.M.B

Methodology: Z.P.L, H. M., J.D.P, M.P., L.B., E.G. F.C. E.M.B

Validation: Z.P.L, H. M., J.D.P, E.M.B

Investigation: Z.P.L., H.M., J.D.P., T.S-M., M.S., J. P-S, M.P., F.D., L.B. C.C., M.G., A.P., L.H. A.S.J., E.G, F.C.

Visualization: Z.P.L, H. M., J.D.P., F.C., E.M.B

Supervision: E.M.B.

Funding acquisition: M.C.C, E.M.B

Writing – original draft: Z.P.L, E.M.B

Writing – review & editing: Z.P.L, H. M., F.C., Y.J., A.T., W.A.P., M-C.C., E.M.B

Competing interests: The authors declare no competing interests.

Data and materials availability: All data are available in the main text or the supplementary materials

Supplementary Materials

Materials and Methods

Figs. S1 to S13

References (44-70)

Movies S1 to S8

Fig. 1. Plasmodesmata formation and ER cell-cell continuity via incomplete cytokinesis in plants. (**A**) Schematic representation of cell plate formation during cytokinesis. (**B**) SBF-SEM image of 4-day-old *Arabidopsis thaliana* root endodermis dividing cells. (**C, E**) Orthogonal projection of a section of cross-wall (C) and mature wall (E) from B, showing plasmodesmata as black holes in the division wall (incomplete cytokinesis). (**D, F**) Plasmodesmata quantification in cross-walls (D) and mature walls (F), n = 11 and n = 35, respectively. (**G**) 3D segmentation from SBF-SEM data in (B) illustrating ER (green) continuity through adjacent cells across plasmodesmata bridges. (**H**) Zoom on cross wall from (G) showing with ER continuity (white arrows) through plasmodesmata (magenta).

Fig. 2. Stabilized plasmodesmata bridges contain ER. (**A**) Batch electron tomography acquisitions along the entire cell plate at fenestrated-sheet (FS, n = 5) and cross-wall (CRW, n = 4) stages (top, overview of the dividing cells; bottom 3D segmentation of the cell plate for stitched tomograms). Cell plate membrane (PM) in magenta, ER in green, yellow arrows point to fenestrae. (**B**) Quantification of fenestrae events presenting continuous ER across, discontinuous ER across or no ER across at fenestrated-sheet and cross-wall stage. n = 76 fenestrae for FS (five complete cell plates) and n = 42 fenestrae for CRW (four complete cell plates). (**C**) Reconstructed tomography sections across fenestrae events and 3D segmentation showing: (I) open fenestrae with continuous ER; (II) open fenestrae with discontinuous ER and (III) closing fenestrae with ER structures flanking the fusion site. Scale bars, 2 µm (A); 100 nm (C).

Fig. 3. The ER creates an energy barrier preventing full fenestrae closure. (**A**) Computational model of energetically metastable plasmodesmata. The presence of ER works against full fenestrae closure (PM sealing) by creating an extra energy barrier (that of ER removal), leading to metastable structure of about 19.5 nm in diameter (ΔF, free energy of the structure. L, longitudinal length of the fenestrae). (**B**) Schematic model of fenestrae contraction and stabilization during cytokinesis from fenestrated-sheet (FS) to cross-wall (CRW) stages. PM term is used for the cell plate membrane. (**C**) Diameter of ER tubes across fenestrae at FS and CRW stages. n = 50 for FS and n = 41 for CRW extracted from electron tomography acquisition from Fig.2. (**D**) Diameter of fenestrae (PM) at FS and CRW stage, n = 76 for FS and n = 42 for CRW extracted from electron tomography acquisition from Fig.2. (**E**) Plotting of fenestrae (PM) diameters together with ER state (continuous, discontinuous, absence, and diameter) during FS and CRW stages.

Fig. 4. MCTPs ER-tethers are necessary for plasmodesmata formation. (**A-B**) CLEM on YFP-MCTP4 expressed in genetically complemented *mctp3/mctp4* mutants in root meristem epidermal cells. (B) enlarged region as in A (outlined white rectangle). Black arrows point to the two plasmodesmata connecting cell a and cell b. Green: YFP-MCTP4; Magenta: PM; CW: cell wall; TEM: transmission electron microscopy. (**C**) airyscan imaging of live Arabidopsis meristem epidermal cells expressing YFP-tagged MCTP3, MCTP4, MCTP6, SYT1, STY5 (green fire blue) under their native promoter; RTN6 under 35S promoter. PM (magenta) is stained by FM4-64. (**D-E**) Quantification of plasmodesmata density on cross-walls and mature walls (number of plasmodesmata/µm^2) in the *A. thaliana* root meristem endodermis cells using SBF-SEM. The bars indicate the mean. Significance was tested using ordinary two tailed Mann-Whitney U-tests (****,

P<0.0001). n = 15 (Col-0), n = 16 *(mctp3/mctp4*), n = 15 (*mctp3/mctp4/mctp6*), n = 10 (*mctp3/mctp4 x UBQ10-YFP-MCTP4 line* #3), n = 10 (mctp3/mctp4 x UBQ10-YFP-MCTP4 line #4) cells for the cross-wall quantification. n = 30 (Col-0), n = 30 (*mctp3/mctp4*), n = 30 (*mctp3/mctp4/mctp6*), n = 20 (*mctp3/mctp4 x UBQ10-YFP-MCTP4* line #3), n = 20 (*mctp3/mctp4 x UBQ10-YFP-MCTP4* line #4) cells for the mature wall quantification. Scale bars, 1 µm (A, B, C, E) or 20 nm (F).

Fig 5. MCTPs accumulate and oligomerize within nascent plasmodesmata late cytokinesis to prevent abscission. (**A**) YFP-MCTP4 time lapse during cytokinesis in the *mctp3/mctp4* complemented *A. thaliana* seedling root epidermal cells. Time 0 indicates the start of cross-wall stage. Note MCTP4 signal starts to accumulate as dots at the onsite of the cross-wall stage. MCTP4 in color coded green fire blue and cell plate in magenta (FM4-64). (**B**) Analyzed by CLEM, YFP-MCTP 'dots' (I) correspond to nascent plasmodesmata (II). (**C**) MCTP4 domain organization and 3D structure. (**D-E**) YFP-MCTP4 mobility during early, late cytokinesis and post cytokinesis, measured by fluorescence recovery after photobleaching (FRAP) in root epidermal dividing cells from *mctp3/mctp4* complemented line. The white squares indicate the photobleaching regions at t = 0. Yellow arrows indicate MCTP4 'dots' that does not recover fluorescent signal after photobleaching. Time is shown in second. Quantification of fluorescence (mean ± SD) and mobile fraction (bars indicate mean) in n = 19 (early cytokinesis) and n = 19 (late cytokinesis) dividing cells. Significance was tested using ordinary two tailed Mann-Whitney U-tests (****, P<0.0001). (**F**) YFP-MCTP4, extracted by digitonin, oligomerizes *in vivo*, as shown by 3-12 % Blue native-PAGE gel. Black arrows point to MCTP4 high-molecular weight complexes in both short (51 s) and long exposed (157 s) blots. Non-specific (NS) indicates non-specific band. Representative results from 3 technical replicates. (**G**) Enrichment of MCTP (ϕ_t=fraction of MCTP covering the ER surface) further stabilizes nascent plasmodesmata bridges by reducing the free energy of the system, which both and depends on both their tethering and ER shaping functions. (**H)** Recapitulative schema. Molecular decision making between abscission and stabilization of constricting fenestrae into plasmodesmata bridges come from the ER and ER-associated MCTPs. Scale bars, 5 µm (A and E), 50 nm (B I, II).

.